Geotechnical Engineering in the XXI Century: Lessons learned and future challenges
N.P. López-Acosta et al. (Eds.)

© 2019 The authors and IOS Press.
This article is published online with Open Access by IOS Press and distributed under the terms of the Creative Commons Attribution Non-Commercial License 4.0 (CC BY-NC 4.0).
doi:10.3233/STAL190054

Sudden Failure of a Soft Soil Subjected to Static and Cyclic Loading

Hernán PATIÑO[a,b,1], Eliana MARTÍNEZ[a] and Rubén GALINDO[a]
[a] *Technical University of Madrid, Spain*
[b] *Colombian Institute of Geotechnical Researches*

Abstract. This paper describes a proposed methodology to evaluate the risk of "sudden failure" that can be experienced by a soft cohesive soil when subject to combined static and dynamic loading. The method is based on the results of a comprehensive experimental research program comprising 155 cyclic simple shear tests. In most tests, prior to the dynamic shear stresses (τ_c), different levels of monotonic bias shear stresses (τ_o) were applied. Laboratory tests were performed on undisturbed specimens recovered at the port of Barcelona, Spain. In general, the results thus obtained indicate that by means of simple correlations among the stiffness modulus (G), the effective vertical consolidation stresses (σ'_{ov}), the cyclic strains (γ_c) and the number of cycles (N), it is possible to combine families of curves that make it possible to evaluate the risk of "sudden failure", for different cyclic shear stress ratios (CSR) equal to (τ_c/σ'_{ov}).

Keywords. Cohesive soils, cyclic load, dynamic, sudden failure.

1. Introduction

Researchers and geotechnical engineers have paid more attention to the study and understanding of granular materials than to the analysis of cohesive materials. This is mainly because most reported failures that are induced by dynamic loads correspond to the performance of seismic action on this type of soil. Thus, potentially dangerous areas are identified as loose and saturated granular soils, where the phenomenon of liquefaction can occur. Liquefaction involves a reduction of the effective stress, caused by sudden increase of pore water pressure, which may even cause total loos of shear strength, so that the ground is not able to withstand any load.

However, in the case of cohesive soils, the phenomenon is different from liquefaction and sudden failure is identified when the strains grow uncontrollably. In general, this failure does not correspond to the situation of null effective stress and should be properly identified to assess the risk of sudden failure. In other words, sudden failure defined herein as sudden onset of large strains, as consequence of partial loss of shear strength.

Some of the research carried out in the last 15 years, related to the dynamic behavior of cohesive soils, have been reported by several researchers [1-19].

[1] Correspondence to: ETSICCP, C/Profesor Aranguren s/n, Madrid 28040, Spain.
E-mail: hernan.patino@upm.es.

2. Description of the equipment used

Laboratory data, which provided experimental support, were conducted with cyclic simple shear test equipment manufactured by an English Company; full description can be found in [20].

3. Material used

The samples for the research program described herein were obtained in a Holocene deltaic deposit, normally consolidated, at a site located in Port of Barcelona in the mouth of the Llobregat River, which discharges into the Mediterranean Sea. Thus, the recovered samples belong to a sedimentary environment composed by intercalations of silt and clay.

Undisturbed samples were recovered from subsoil at the Port of Barcelona, from exploratory borings SA-1 and SA-2 in particular. These borings were advanced from the deck of Prat Pier (41º19'34"N,2º08'41"E). The exploration method was mud rotary and Shelby tube was used to extract the samples.

According [17], the generalized stratigraphic profile of the area close to the Prat Llobregat Pier comprises:

- Stratum 1: Deposit of marine origin, constituted by silt and clay varying in colour from brown to grey, with dark shades upon an increase of the organic matter content. Stratified layers of sand and of sandy silt are found in the upper part. The thickness of this layer is approximately 50 m.
- Stratum 2: Gravel and sand with traces of silt. This layer has an approximate thickness of 7 meters.
- Stratum 3: Clays with properties similar to those of layer 1, but with a lower compressibility. The maximum thickness of this stratum was 14 m.
- Stratum 4: Gravel and sand interspersed with clay. Its thickness exceeds 40 m.

The samples tested for this investigation were collected within the upper portion of Stratum 1 between 29 and 50 m depth. The tested soil according to the Casagrande's Plasticity Chart, can be classified as silty clays and clayed silt of medium to low plasticity. Mineralogical content is as follows: calcite 42%, quartz 31%, chlorite 13%, albite 9%, and muscovite 5%.

The index properties of the samples tested are presented in Table 1.

Table 1. Summary of index properties.

Parameter	Unit	No. of data	Range
Natural unit weight	kN/m^3	154	17.8-21.3
Natural moisture	%	154	15-44
Content of fines	%	154	86-100
D< 2 m	%	14	14-41
Liquid limit	%	39	24-45
Plastic limit	%	39	16-25
Plasticity index	%	39	6-24
Specific gravity	-	36	2.71-2.80

4. Experimental program

In addition to laboratory index tests, the program included 155 cyclic simple shear tests, in which prior to the dynamic shear stresses different levels of monotonic shear stresses were applied. The total number of cyclic simple shear tests is a result of the combination of τ_c/σ'_{ov} values equal to 10, 15, 20 and 25% and CSR values equal to 0, 10, 15, 20 and 25%.

To eradicate factors that may affect the behavior of the studied soil, in addition to the combination of static and cyclic stresses, the following conditions were established for all of the tests: undisturbed samples, specimens of 7 cm of diameter and 1.91 cm of height, consolidation stress equal to the in-situ effective vertical stress (σ'_{ov}), undrained conditions and evaluation of the pore water pressure generated, stress controlled during the cyclic stage and sinusoidal wave with an amplitude equal to the cyclic stress ($\Delta\tau_c$) evaluated as a percentage of σ'_{ov} and frequency of 0.1 Hz.

5. Results

5.1. Modulus (G) as a function of the number of cycles (N)

Figures 1a and 1b plot the shear modulus (G) for cyclic loading normalized with respect to the in-situ effective vertical stress (σ'_{ov}) and the number of cycles (N) for cyclic strains (γ_c) from 1–14%, is depicted in Figure.1a) (where the case unbiased cyclic loading $\tau_o/\sigma'_{ov}=0$ is shown). Herein, G is defined as the secant shear modulus obtained in the last loading cycle.

If vertical sections are plotted in Figure.1a), through the ordinate values corresponding to 1, 10, 100 and 1000 cycles, the trends of variation of the dynamic stiffness modulus (G) normalized with respect to the in-situ effective vertical stress (σ'_{ov}) are obtained in terms of the cyclic strains (γ_c) and the number of cycles (N) of 1, 10, 100 and 1000, as shown in Figure. 1b).

From this figure, the following expression can be established as follows:

$$\frac{G}{\sigma'_{ov}} = C_1 \cdot (\gamma_c)^{C_2} \tag{1}$$

where C_1 and C_2 are empirical specific constants of the material tested.

For the same value of the normalized monotonic stress (τ_o/σ'_{ov}), it is possible to replace the constants C_1 and C_2 by correlations based on the number of cycles in expression (1). This evaluation, although approximate in nature, can be made with the following equation:

$$\frac{G}{\sigma'_{ov}} = (C_3 \cdot N^{C_4}) \cdot (\gamma_c)^{(C_5 \cdot lnN + C_6)} \tag{2}$$

where C_3, C_4, C_5 and C_6 are empirical specific constants of the material tested.

The values of the empirical constants in this investigation are included in Table 2.

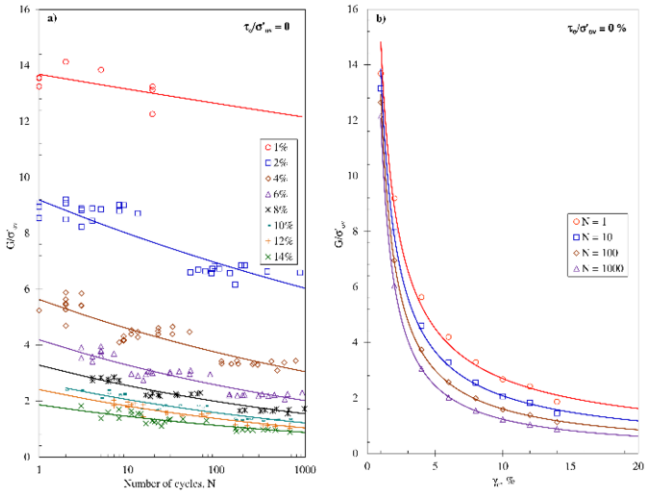


Figure 1. a) Variation of G/σ'_{ov} as a function of the number of cycles and of the cyclic strain corresponding to unbiased cyclic loading $\tau_o/\sigma'_{ov}=0$. b) Vertical sections in a) for values of N equal to 1, 10, 100 and 1000.

5.2. Effective vertical stress (σ'_v) as a function of the number of cycles (N).

The experimental results included in Figure 2a) correspond to the typical variation trends that were found in the effective vertical stress (σ'_v) normalized with respect to the in-situ effective vertical stress (σ'_{ov}) as a function of the number of cycles (N) and for cyclic strains from 1–14%.

In the same manner as above, if vertical sections are plotted in Figure. 2 a) through the ordinate values that correspond to 1, 10, 100 and 1000 cycles, Figure 2 b) can be obtained. Thus, the following expression can be established by mathematical fit:

$$\frac{\sigma'_v}{\sigma'_{ov}} = D_1 \cdot (\gamma_c)^{D_2} \tag{3}$$

where D_1 and D_2 are empirical specific constants of the material tested.. For the same value of ($\tau_o/\ \sigma_{ov}$), it is possible to replace the constants D_1 and D_2 by correlations based on the number of cycles using the following novel mathematical expression:

$$\frac{G}{\sigma'_{ov}} = (D_3 \cdot N^{D_4}) \cdot (\gamma_c)^{(D_5 \cdot lnN + D_6)} \tag{4}$$

where D_3, D_4, D_5 and D_6 are empirical specific constants of the material tested.

The values of the empirical constants in (3) and (4) are shown in Table 2.

Table 2. Summary of values of the empirical constants in (1), (2), (3) and (4).

τ_o/σ'_{ov}	N	C_1	C_2	C_3	C_4	C_5	C_6	D_1	D_2	D_3	D_4	D_5	D_6
0	1	14.83	-0.74					94.35	-0.32				
0	10	13.84	-0.82	15	-0.03	-0.04	-0.74	70.11	-0.40	96	-0.13	-0.04	-0.32
0	100	12.93	-0.91					52.09	-0.48				
0	1000	12.07	-0.99					38.70	-0.56				

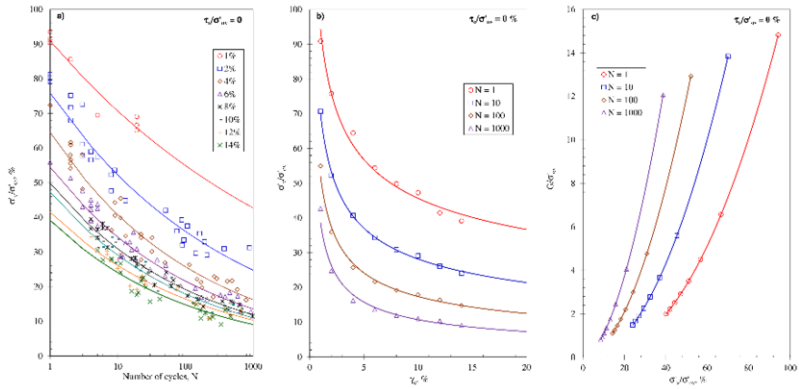


Figure 2. a) Variation of σ'_v/σ'_{ov} as a function of the number of cycles and of the cyclic strain corresponding to unbiased cyclic loading $\tau_o/\sigma'_{ov}=0$. b) Vertical sections in a) for values of N equal to 1, 10, 100 and 1000. c) Variation of G/σ'_{ov} as a function of σ'_v/σ'_{ov}.

5.3. Modulus (G) as a function of the effective vertical stress (σ'_v)

Combining expressions (2) and (4), the correlation between the shear modulus of stiffness and the effective vertical stress can be found for each number of cycles:

$$\frac{G}{\sigma'_{ov}} = E_1 \cdot \left(\frac{\sigma'_v}{\sigma'_{ov}}\right)^{E_2} \tag{5}$$

where E_1 and E_2 are empirical constants that can also be obtained as a function of the number of cycles with the following proposed expression:

$$\frac{G}{\sigma'_{ov}} = (E_3 \cdot N^{E_4}) \cdot \left(\frac{\sigma'_v}{\sigma'_{ov}}\right)^{(E_5 \cdot lnN + E_6)} \tag{6}$$

where E_3, E_4, E_5 and E_6 are empirical specific constants of the material tested..

The values of the empirical constants in (5) and (6) are shown in Table 3.

Table 3. Summary of values of the empirical constants in (5) and (6).

τ_o/σ'_{ov} (%)	N	E_1	E_2	E_3	E_4	E_5	E_6
0	1	0.0003	2.35	0.0004	0.59	-0.08	-2.31
0	10	0.002	2.08				
0	100	0.007	1.91				
0	1000	0.018	1.80				

The results obtained from expression (6) are presented in Figure 3c) and correspond to typical trends of variation determined in this investigation for $\tau_o/\sigma'_{ov}=0$.

The trends of variation in the orthogonal spaces G/σ'_{ov}-γ_c, σ'_v/σ'_{ov}-γ_c and G/σ'_{ov}-σ'_v/σ'_{ov} are the source, for each value of τ_o/σ'_{ov}, of the curves identified with the letters A, B, C, and D in the three-dimensional space (σ'_v/σ'_{ov}, γ_c, G/σ'_{ov}) shown in Figure 3a).

If the three-dimensional space (σ'_v/σ'_{ov}, γ_c, G/σ'_{ov}) in Figure. 3a) includes only curves A, B, C, and D without their respective projections into the orthogonal planes and if

curves that identify the cyclic strains are included, the space surface indicated in Figure. 3b) is obtained.

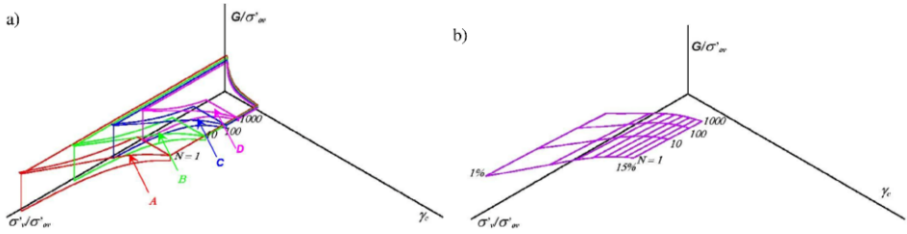


Figure. 3. Three-dimensional representation of: a) the trends of variation of γ_c, σ'_v/σ'_{ov} and G/σ'_{ov}, for different numbers of cycles and $\tau_o/\sigma'_{ov}=0$ and b) the surface in the space that contains, for each value of τ_o/σ'_{ov}, the possible combinations between parameters G, σ'_{ov}, γ_c, σ'_v and N. The surface correspond to $\tau_o/\sigma'_{ov}=0$.

5.4. Cyclic stress (τ_c) as a function of the effective vertical stress (σ'_v)

When transforming the vertical axis of Figure 3 to develop a representation in terms of the cyclic stress (τ_c) rather than in terms of the shear modulus of stiffness and inverting the direction of the horizontal axis, the graphs plotted in Figure 4 can be obtained for each value of τ_o/σ'_{ov} (this transformation is possible because the dynamic stiffness modulus (G) refers only to the cyclical part of the load and therefore $\tau_c=G\gamma_c$).

From these graphs, plotted in terms of the effective stress or as a function of the pore water pressure, it is possible to carry out the analysis described in the following paragraphs. The following analysis is valid for the condition in which $\tau_o/\sigma'_{ov}=0$.

For the liquefaction phenomenon to develop in loose granular materials, the pore water pressure generated during dynamic loading must increase until the effective stress decreases to zero. However, in the cohesive soil studied, it suffices that the effective stress decreases by 20%, that the cyclic stress becomes 20% of the effective vertical stress and that the soil is subjected to 20 cycles for the soil to experience shear strains of 15% and, therefore, a sudden failure. Comparatively, this condition could be regarded as the most critical.

If the cyclic stress is approximately 30% of the in-situ effective vertical stress in a cycle, the resulting pore water pressure may reach close to 60% of the in-situ effective vertical stress. This may lead to a sudden failure (Figure 4a)) for $\tau_o/\sigma'_{ov}=0$.

For cyclic stresses less than 12% of the in-situ effective vertical stress and pore water pressures less than 60% of the in-situ effective vertical stress, the risk of failure under dynamic loading is practically zero because the maximum cyclic strains become 1% (Figure 4a)) for $\tau_o/\sigma'_{ov}=0$. With relatively low cyclic stresses, approximately 12% of the in-situ effective vertical stress, if the generated pore water pressure exceeds 60% of the in-situ effective vertical stress, there is almost no possibility of the occurrence of a sudden failure under few cycles, but the soil will experience higher strains when subjected to a relatively high number of cycles (Figure 4a)) for $\tau_o/\sigma'_{ov}=0$.

Under the conditions $\tau_o/\sigma'_{ov}=0$, $\tau_o/\sigma'_{ov}+\tau_c/\sigma'_{ov}=30\%$ and $\sigma'_v/\sigma'_{ov}=40\%$ (Figure 4a)), the soil experiences a cyclic strain of 15% in one cycle.

The condition $\sigma'_v/\sigma'_{ov}=40\%$ apparently defines the threshold in which cyclic strains increase, as σ'_v/σ'_{ov} is reduced, even for low cyclic stresses. It can be observed in

Figure 4a) for τ_o/σ'_{ov}=0%, that for τ_c/σ'_{ov}=12% and σ'_v/σ'_{ov} > 40%, the cyclic strains are less than 1%, but if σ'_v/σ'_{ov} < 40%, the cyclic strains may reach 15%, even for low levels of cyclic stresses (τ_c/σ'_{ov}=12%).

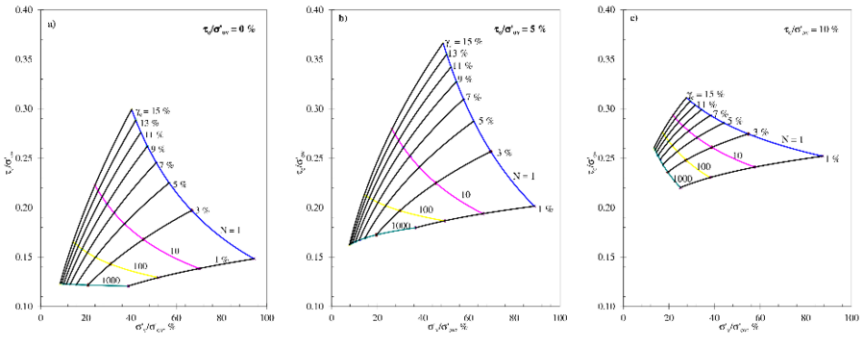


Figure 4. Graphs to evaluate the risk of sudden failure of the cohesive deposit under study.

6. Conclusions

From complete laboratory research conducted on soil samples from the subsoil of the Port of Barcelona at the mouth of the Llobregat River, a methodology for studying the risk of sudden failure is proposed. This methodology involves testing different combinations of static and cyclic stresses using the cyclic simple shear test, obtaining formulas and generating graphs of the risk of sudden failure. This approach may be appropriate for the dynamic study of soils in cohesive media, summarizing the main variables and influencing factors and allowing proper analysis of the degradation of the shear stiffness module, influence of static shear stress, pore water pressure generation and evolution with the number of cycles.

Regarding stresses, it is convenient to consider not only the variation of the cyclic shear stress (τ_c) but also the existing static shear stress (τ_o) prior to the application of any type of dynamic loading because both the static and the cyclic stresses, which act independently, affect the behavior, but the combination of both is even more critical. The most important aspects to be highlighted are summarized as follows:

It can be expressed that, regardless of the magnitude of τ_o/σ'_{ov}, the responsible factor for the sudden failure is actually the magnitude of $\Delta\tau_c/\sigma'_{ov}$. Thus, large cyclic and permanent strains occur after a reduced number of cycles in this condition.

The pore water pressure generated during cyclic loading controls the risk of sudden failure and the development of permanent strains. For the same summation of stresses $\tau_o/\sigma'_{ov}+\tau_c/\sigma'_{ov}$, the soil experiences sudden failure with low monotonic shear stresses (τ_o) and high cyclic shear stresses ($\Delta\tau_c$).

For the soil studied, it is sufficient for the effective stresses (σ'_v) to decrease to 30% of the in-situ effective vertical stress (σ'_{ov}) for sudden failure to occur; this is a very critical condition compared with the liquefaction phenomenon experienced by loose granular materials when the effective stresses (σ'_v) decrease to practically zero.

As applicable to the soil studied, simple mathematical expressions approximately correlate to G/σ'_{ov}, σ'_v/σ'_{ov} and τ_c as a function of the number of cycles. The proposed expressions to fit the experimental results are novel.

For each ratio τ_o/σ'_{ov} it is possible to represent the trends of variation of G/σ'_{ov}, σ'_v/σ'_{ov} and τ_c in a three-dimensional space among themselves and as a function of the number of cycles (N) and to discover the spatial surface where the possible combinations of G/σ'_{ov}, σ'_v/σ'_{ov} and τ_c and N are located. These possible combinations, if projected in the plane G/σ'_{ov}, σ'_v/σ'_{ov}, are the source of graphical presentations that make it possible to evaluate the risk of sudden failure (Figure 4).

References

[1] Boulanger R. W., Idriss I. M. (2004). "Evaluating the potential for liquefaction or cyclic failure of silt sand clays", University of California at Davis.
[2] Martin I. J. R., Olgun C. G., Mitchell J. K. & Durgunoglu H. T. (2004) "High-modulus columns for liquefaction mitigation", Journal of Geotechnical and Geoenvironmental Engineering, 130(6): 561-571.
[3] Santagata M, Germaine J. T. & Ladd C. C. (2005). "Factors affecting the initial stiffness of cohesive soils", Journal of Geotechnical and Geoenvironmental Engineering, 131(4): 430-41.
[4] Boulanger R. W. & Idriss I. M. (2007). "Evaluation of cyclic softening in silts and clays", Journal of Geotechnical and Geoenvironmental Engineering, 133(6): 641-652.
[5] Finno R. J. & Cho W. (2007). "Recent stress history effects on compressible Chicago glacial clays", Journal of Geotechnical and Geoenvironmental Engineering, 137(3): 197-207.
[6] Chang W. J. & Hong M. L. (2008). "Effects of clay content on liquefaction characteristics of gap- graded clayey sands", Soils and Foundations, 48(1): 101-14.
[7] Chu D. B., Stewart J. P., Boulanger R. W. & Lin P. S. (2008). "Cyclic softening of low-plasticity clay and its effect on seismic foundation performance", Journal of Geotechnical and Geoenvironmental Engineering, 134(11): 1595-1608.
[8] Patiño H. (2009). "Influencia de la combinación de tensiones tangenciales estáticas y cíclicas en la evaluación de parámetros dinámicos de un suelo cohesive, PhD Thesis, ETSICCP-UPM.
[9] Soroush A. & Soltani-Jigheh H. (2009) "Pre- and post-cyclic behavior of mixed clayey soils", Canadian Geotechnical Journal, 46(2): 115-28.
[10] Huang A. B. & Chuang S. Y. (2011). "Correlating cyclic strength with fines contents through state parameters", Soils and Foundations, 51(6): 991-1001.
[11] Patiño H., Soriano A. and Gonzalez J. (2013). "Failure of a soft cohesive soil subjected to combined static and cyclic loading", Soils and Foundations, 53(6): 910-922.
[12] Subramaniam P. & Banerjee S. (2013). "Shear modulus degradation model for cohesive soils", Soil Dynamics and Earthquake Engineering, 53: 210-216.
[13] Tsai C., Mejia L. H. and Meymand P. (2014). "A strain-based procedure to estimate strength softening in saturated clays during earthquakes", Soil Dynamics and Earthquake Engineering, 66: 191-8.
[14] El Takch A., Sadrekarimi A. and El Naggar H. (2016). "Cyclic resistance and liquefaction behavior of silt and sandy silt soils", Soil Dynamics and Earthquake Engineering, 83: 98-109.
[15] Kim U., Kim D. and Zhuang L. (2016). "Influence of fines content on the undrained cyclic shear strength of sand–clay mixtures", Soil Dynamics and Earthquake Engineering, 83: 124-34.
[16] Martínez, E., Patiño, H. and Galindo R. (2017). "Evaluation of the risk of sudden failure of cohesive soil subjected to cyclic loading", Soil Dynamics and Earthquake Engineering, 92: 419-432.
[17] Alonso E., Gens A., Madrid R. and Uzcanga J. (2007). "The soft foundation soils of new breakwaters at the port of Barcelona, Proceedings of the 14th ECSMFE: 1765-1770.
[18] Zergoun, M. & Vaid, Y. (1994). "Effective stress response of clay to undrained cyclic loading", Canadian Geotechnical Journal, Vol. 31, Nº 5: 714 –727.
[19] Sanin M.V. & Wijewickreme D. (2006). "Cyclic shear response of channel-fill Fraser River Delta silt", Soil Dynamics and Earthquake Engineering, 26(9): 854-869, DOI: 10.1016/j.soildyn.2005.12.006
[20] https://www.controls-group.com/eng/soil-mechanics-testing-equipment/cyclic-simple-shear.php